PHYSICAL REVIEW B **103**, 054435 (2021)

Domain-wall dynamics in multisegmented Ni/Co nanowires

V. O. Dolocan [*]
Aix-Marseille Université, CNRS, IM2NP UMR7334, F-13397 Marseille Cedex 20, France

(Received 2 December 2020; revised 10 February 2021; accepted 15 February 2021; published 23 February 2021)

The current-induced motion of transverse magnetic domain walls (DWs) in a multisegmented Co/Ni nanowire is investigated numerically. We find that the phase diagram current pulse length magnitude presents a rare diversity of behaviors depending on the segment's length and material parameters. We show that by changing only the pulse shape, in a range of parameters we obtain the controlled motion of the DW with or without polarity change. The polarity change arises in the simplest case from the birth and propagation of an antivortex along the width of the nanowire. The antivortex can be displaced over long distances depending on the pulse characteristics and boundary conditions. The systematic motion of the DW with polarity flip is found to be stable at room temperature. Moreover, by modifying the material parameters through alloying, the phase diagram can be engineered, decreasing the depinning current and paving the way for storage or logic applications.

DOI: 10.1103/PhysRevB.103.054435

I. INTRODUCTION

An increasing number of magnetic nanostructures are studied nowadays for their storage or logic properties. Functional devices are designed that use the magnetic domains as digital bits which are displaced in a controlled manner inside the nanostructure. These devices take advantage of the domain wall (DW) motion induced by a magnetic field or a spin polarized electric current [1,2] in a flat or cylindrical nanowire. The central ingredient is the proper manipulation of the DW's motion between well-defined positions (pinning centers) in the nanowire in a reproducible manner [3,4]. Several approaches were used to tailor the DW energy landscape like artificial constrictions or protuberances [5–9], bending [10], or local modifications of the magnetic properties like anisotropy or the saturation magnetization [11–13].

Recently, multisegmented nanowires (sometimes referred to as multilayered nanowires), which are formed by alternating regions of different composition and structure along the longitudinal axis, were investigated for spintronic applications. Ferromagnetic (FM)/FM [14,15] or FM/nonmagnetic (NM) [16] multisegmented nanowires were studied for shift registers [17], magnetic nano-oscillators [18], and flexible spin caloritronic devices [19]. In most cases, cylindrical nanowires were fabricated by electrochemical deposition in alumina templates [20], which readily allows for modifications of geometrical aspect or material properties. Metallic FM/FM multisegmented cylindrical nanowires composed of Co and Ni segments were shown experimentally to efficiently pin the vortex DWs at the Co/Ni interface [15]. It was shown that individual Co nanowires can be prepared as single crystals with *hcp* structure and controlled easy-axis orientation [21]. A FM nanowire with segments of different materials and different orientations of the magnetization easy axis can therefore be easily engineered. However, the complex magnetic states (multivortex) observed in these wires and the DW dynamics are not completely understood.

In this paper, we address this issue by studying the systematic motion of a magnetic transverse DW in a Co/Ni multisegmented nanostrip (flat nanowire) when submitted to ultrashort spin-polarized current pulses at low and room temperature. When the magnetocristalline anisotropy easy axis is oriented out of plane for the Co segments, a complex periodic pinning potential is created in which an individual transverse DW moves between pinning sites (the Ni regions) for a large range of geometrical characteristics (width/length/number) of segments. The stray field generated at the interfaces between Co and Ni regions strongly deform the DW, which behaves like a string in a tilted washboard potential [22]. When a current pulse is applied, the DW is tilted out of plane (tilting angle ψ), which is usually suppressed by the effective wall anisotropy $K_\perp$. A small variation in $K_\perp$ can cause an exponentially large change in ψ at the segment edges [23] and, for certain pulse characteristics and material parameters, an antivortex appears [24] that can traverse the nanostrip width, switching the transverse DW polarity. More complex structures can appear as a vortex-antivortex pair depending on the exchange energy variation and boundary conditions at the interfaces. We show that by varying only the current pulse shape, in a certain parameter range, the transverse DW can be reliably displaced with or without polarity change with potential applications for storage devices. Our results show that the systematic DW displacement between pinning regions with a polarity switch is stable at room temperature in a Co/Ni multisegmented nanowire. We also determine the impact of the material parameter variation, for example, by alloying, on the depinning current and phase diagrams. A 1D model is developed that agrees with the numerical one only in the parameter range where no vortex-antivortex structures appear. Our study brings physical insight into DW motion in multisegmented nanowires and could lead to future theoretical and applied studies.

This paper is organized as follows. In Sec. II, we present the numerical simulations and stochastic 1D model used to

---

[*] voicu.dolocan@im2np.fr

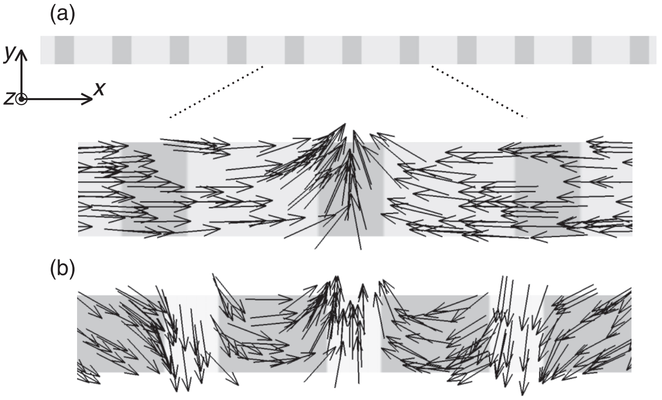

FIG. 1. (a) Multisegmented Co/Ni nanowire with an in-plane transverse DW. The Ni regions (40 nm length) are shaded and the Co regions (80 nm length) have a magnetocrystalline anisotropy along the z axis. The arrows indicate the direction of the magnetization. The enlarged section shows the central regions with the transverse domain wall. (b) Expanded part of the multisegmented nanowire when the Co regions have a magnetocrystalline anisotropy along the y axis. The length of the regions have been inverted: Co regions of 40 nm and Ni regions of 80 nm. The nanowire is 1300 nm long, 60 nm wide, and 5 nm thick.

calculate the DW displacement. In Sec. III, we compute and investigate the phase diagram of the DW dynamics in an infinite nanostrip at $T = 0$ K and at room temperature. Discussion and concluding remarks are presented in Sec. IV.

II. MODEL

The dynamics of the DWs is governed by the Gilbert form of the Landau-Lifschitz equation (LLG) with adiabatic and nonadiabatic spin-transfer torques (STTs) [25],

$$\begin{aligned}\dot{\mathbf{m}} = &-\gamma_0 \mathbf{m}\times\mathbf{H}_{\text{eff}} + \alpha(\mathbf{m}\times\dot{\mathbf{m}})\\ &-(\mathbf{u}\cdot\nabla)\mathbf{m} + \beta\mathbf{m}\times(\mathbf{u}\cdot\nabla)\mathbf{m},\end{aligned} \tag{1}$$

where $\mathbf{m}$ is the normalized magnetization, γ_0 is the gyromagnetic ratio, $\mathbf{u} = \mathbf{j}_e P\mu_B/eM_s$ is the spin drift velocity, P the spin polarization of conduction electrons (taken as 0.7 in numerical simulations), μ_B the Bohr magneton, and $\mathbf{j}_e$ the applied current density. The temperature is added to the LLG equation in the form of a thermal field with zero average and uncorrelated in time and space.

We study the dynamics of a transverse DW in a multisegmented nanostrip of Co and Ni regions. The type of DW in confined nanostructures depends on the nanostrip dimensions [26]. The length of the regions/segments (along the longitudinal x axis) is varied between 20 and 40 nm for Ni and between 50 nm and 90 nm for Co. The width (along y axis) and the thickness of the nanostrip are kept constant at 60 nm and, respectively, at 5 nm, while the total strip length is varied around the value of 1300 nm to ensure that the end regions are always made of Co [Fig. 1(a)]. The following parameters are used for Ni: saturation magnetization $\mathrm{M}_s = 477$ kA/m, exchange stiffness parameter $\mathrm{A} = 8.6$ pJ/m, and damping parameter $\alpha = 0.05$, and for Co: saturation magnetization $\mathrm{M}_s = 1400$ kA/m, exchange stiffness parameter $\mathrm{A} = 28.1$ pJ/m, damping parameter $\alpha = 0.005$, and uniaxial magnetocrystalline anisotropy (MCA) $\mathrm{K}_u = 4.5\times10^5\ \mathrm{J/m^3}$ [27] if not specified otherwise. When the Co MCA easy axis is directed along the perpendicular z axis, the transverse DW is pinned in the Ni regions for the geometrical dimensions of the regions chosen [see Fig. 1(a)], with the magnetization in plane. When the Co MCA is directed along the transverse y-axis a single DW is no longer a stable state and the DWs are pinned in the Co regions as shown in Fig. 1(b). As the reliable control of the DW position is a prerequisite for memory applications, only the case with the Co regions having perpendicular z-axis MCA is studied below.

A series of periodic spin-polarized current pulses are applied along the stripe longitudinal axis (x direction) to displace the DW, which is initiated in the central Ni region. The current pulse has a trapezoidal geometry with t_r, t_s, and t_f the rise, stable, and fall times [3]. The periodic pulses are separated by t_z, the zero-current time which ensures that the DW reaches its equilibrium position before another pulse is applied. The nonadiabatic parameter is set to $\beta = 2\alpha$ if not specified otherwise.

The DW dynamics was computed mainly using 3D micromagnetic simulations with the MUMAX3 package [28]; some simulations were also conducted with the OOMMF package [29]. The strip was discretized into a mesh with a cell size of $2\times3\times2.5\,\mathrm{nm}^3$, inferior to the exchange length. A one-dimensional model [30] was also developed to understand the DW displacement in the multisegmented wire. The analytical equations of motion used are based on the 1D model of the DW (collective coordinates: average DW center position X and azimuthal angle ψ) [31,32],

$$\begin{aligned}(1+\alpha^2)\dot{X} = &-\frac{\alpha\gamma\Delta}{2\mu_0 M_s S}\frac{\partial E}{\partial X} + \frac{\gamma\Delta}{\mu_0 M_s}K_\perp\sin 2\psi\\ &+ qp\frac{\gamma}{2\mu_0 M_s S}\frac{\partial E}{\partial\psi} + (1+\alpha\beta)u + \eta_\psi - \alpha\eta_X,\\ (1+\alpha^2)\dot{\psi} = &-qp\frac{\gamma}{2\mu_0 M_s S}\frac{\partial E}{\partial X} - \frac{\gamma\alpha}{\mu_0 M_s}K_\perp\sin 2\psi\\ &-\frac{\alpha\gamma}{2\Delta\mu_0 M_s S}\frac{\partial E}{\partial\psi} + qp\frac{\beta-\alpha}{\Delta}u + \eta_X + \alpha\eta_\psi,\end{aligned} \tag{2}$$

with Δ the DW width, $\mathrm{K}_\perp$ the transverse anisotropy, η_X and η_ψ represent stochastic Gaussian noise with zero mean value and correlations $\langle\eta_i(t)\eta_j(t')\rangle = (2\alpha k_B T)/(\mu_0 M_s\Delta S)\delta_{ij}\delta(t-t')$. E is the potential energy of the DW that includes the internal energy and the pinning energy. The azimuthal angle of the DW ψ represents the conjugate momentum in the Lagrangian formulation. $q = \frac{1}{\pi}\int \mathrm{d}x\partial_x\psi = \pm1$ represents the chirality or the topological charge of the DW and is related to the direction of rotation of the in-plane magnetization when traversing the DW and $p = \pm1$ represents the direction of the magnetization at the DW center along the y axis (width). The product $Q = q\cdot p$ is always equal to $+1$ for a head-to-head DW and to -1 for a tail-to-tail DW.

In the present situation, the DW moves in an effective pinning potential that arises due to the magnetic parameters variation between the segments. The 1D model still gives

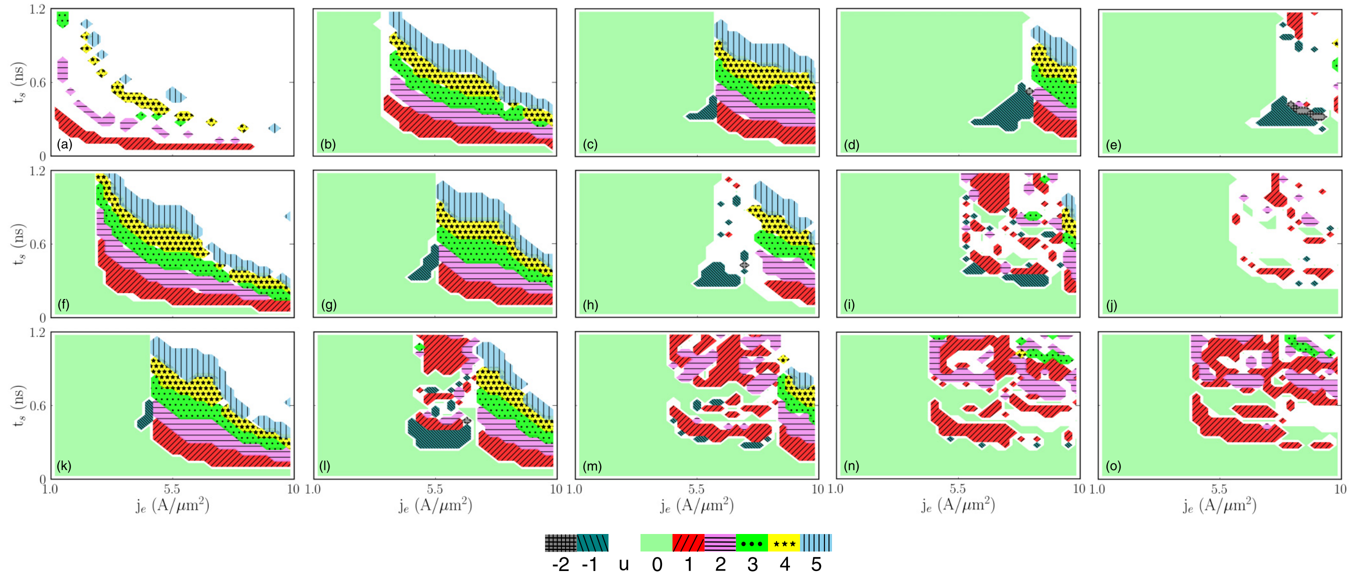

FIG. 2. Micromagnetic phase diagrams (pulse stable time—pulse amplitude) of DW motion under a periodic current pulse in a multisegmented Ni/Co nanowire at $T = 0$ K. The periodic pulse is formed of two identical current pulses of opposite amplitude (forward-backward motion) separated by a waiting time of 5 ns. The length of the Ni and Co regions is varied as—from the top row to the bottom row—the Ni region's length increases from 20 nm (top row) to 40 nm (bottom row) in steps of 10 nm, while the Co region's length increases from left column to right column from 50 nm (left column) to 90 nm (right column) in steps of 10 nm. The thickness of the nanowire is 5 nm and its total length is around 1300 nm (varies slightly to always have Co regions at the ends). The observed DW motion is classified in bands numbered as follows: positive bands correspond to the DW moving in the direction of the electron flow, negative numbers to the DW moving contrary to the electron flow, zero state correspond to the DW staying pinned at initial position, and u to the unintended states in which the DW does not come back to the initial state after the periodic pulse.

good quantitative results (see Ref. [33]), if the azimuthal angle ψ stays well below $\pi/4$. The pinning potential can be determined from micromagnetic simulations together with the numerical integration of the DW energy, allowing for continuous x-axis variation of the material parameters (K, A, M_s, α, β) [12,13] contrary to the micromagnetic model where an abrupt transition between segments is considered excepting the exchange energy (the details of the 1D calculation are presented elsewhere). One parameter that varies locally and can introduce numeric artifacts near interfaces is the exchange energy calculation. In its usual implementations, the exchange energy is approximated between nearest or second-nearest neighbors or interpolated between nearest grid points with the Neumann or Dirichlet boundary conditions [34]. The interfaces can lead to singularities in the magnetization due to a jump in the exchange stiffness A and its effect was studied for some time in connection with grain boundary effects [35,36]. The effective exchange between adjacent pairs of atoms is usually overestimated, particularly in soft magnets when considering the same effective exchange strength over the interface (see Ref. [35] and references therein). In micromagnetic packages, the effective exchange interaction is usually assumed identical on both sides of the interface and calculated by default as a harmonic mean of the values on each side of the interface. A reduced interface exchange may be closer to reality as a real interface may have impurities or mixing phases or be amorphous and was considered below. The details of the exchange stiffness variation in the interface region are described in the Supplemental Material [33].

III. RESULTS

In this section, we study the impact on the DW dynamics of the segment's length and material parameter variation at zero and room temperature. The phase diagram (stable time t_s—current amplitude j_e) obtained when periodic current pulses are applied shows a rich variety of stable states, including systematic displacement with or without DW polarity change.

A. Influence of the segment's length on the phase diagrams at $T = 0$ K

To describe the DW dynamics in a Co/Ni multisegmented nanowire [Fig. 1(a)], we use the analysis previously used for the DW dynamics in a notched nanowire [3,4]. A transverse DW pinned in a Ni region in the center of the nanowire is submitted to a series of periodic trapezoidal spin-polarized current pulses. The Ni regions represent the pinning sites for DW displacement. For a reliable control of DW propagation, the DW should move forward and backward to the same position after a periodic current pulse. The current pulses are varied in length, amplitude, or shape and the DW motion is extracted after several periodic current pulses. The relative DW position, after the series of periodic pulses, is represented in a phase diagram (stable time t_s—current amplitude j_e). The regular DW displacements were shown to form bands depending on the pulse characteristics in notched nanowires [3,4].

In Fig. 2, the influence of the segments length variation on the phase diagram is shown at $T = 0$ K. The Ni segments were varied between 20 and 40 nm (top row to bottom row),

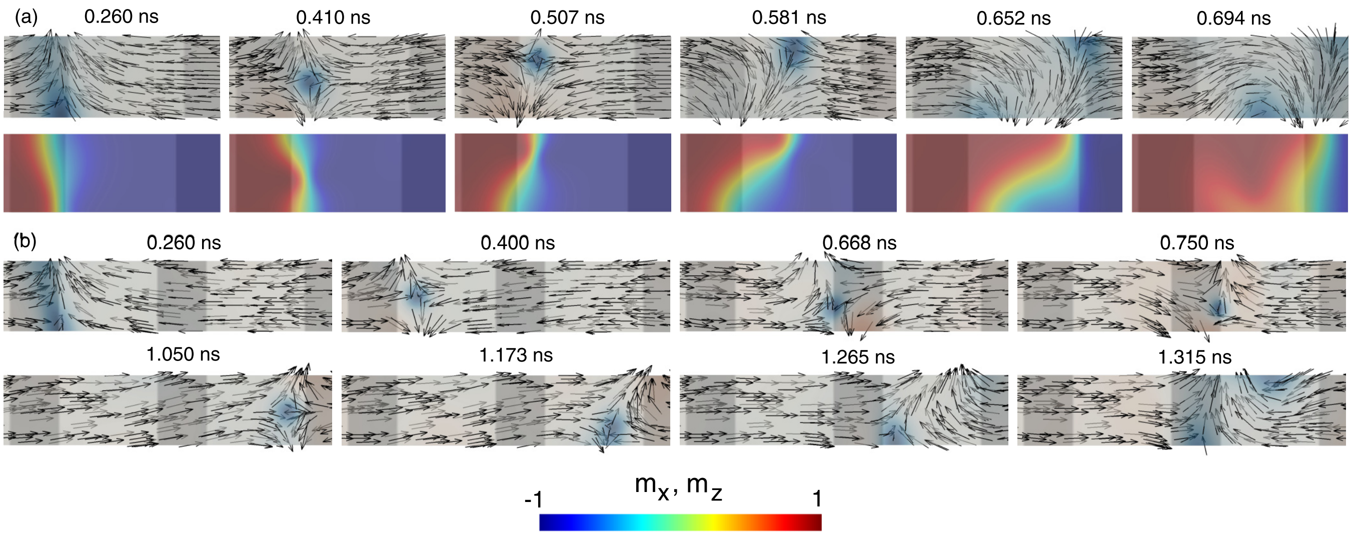

FIG. 3. DW displacement in a 40-nm Ni/80-nm Co segmented nanowire under a current pulse when $t_s = 400$ ps, $j_e = 5.5$ A/μm^2 (a) or $t_s = 1050$ ps, $j_e = 6.4$ A/μm^2 (b) was applied. Both cases correspond to a state +1. The Ni regions are indicated by darker colors. In panel (a), an antivortex is observed crossing the nanowire width (first row, blue circle) while the TDW changes polarity when moving to the nearest Ni region. In panel (b), the antivortex does not cross the nanowire width and is expelled on the same edge it entered. The TDW does not change its polarity when moving to the nearest Ni region. The second row in panel (a) shows the m_x component of magnetization, illustrating the DW deformation in the process.

while the Co segments were varied between 50 and 90 nm (left column to right column). The bands were indexed as follows: band 0 if the DW stays pinned in the initial Ni segment, band +1 if the DW was displaced periodically to the nearest-neighbor Ni segment in the direction of the STT and band −1 if the DW was displaced to the nearest-neighbor Ni segment in the opposite direction of the STT. The superior bands (±-2 etc.) correspond to the DW displacement between the initial pinning site and the second neighboring site and so on. The u state represents an unintended state where the DW does not move periodically back and forth to the initial pinning site or depins completely.

The pinning potential varies strongly with the segment's length [33]. For a small length, the pinning barrier is small and the DW can move easily between the pinning sites as shown in Fig. 2(a). In this case, the DW depins easily and the bands are thin and a reliable control cannot be achieved. Increasing the Ni or Co segment length by 10 nm strongly increases the stability and the band width (Figs. 2(b) and 2(f)). The pinning potential of the Ni segments becomes important as soon as the segment width increases above the DW width (25 nm in Ni). Increasing the Ni width even more diminishes the slope of the pinning potential without a clear modification of the pinning barrier height (details in Ref. [33]). Increasing the Co length increases the barrier height but not the pinning potential slope. The depinning current has a complex dependence on the Ni and Co segment length. It increases with increasing Co or Ni length as long as the DW motion forms regular bands in the phase diagram. Starting from (20-nm Ni)/(90-nm Co) (Fig. 2(e)), (30 nm Ni)/(70 nm Co) (Fig. 2(h)) and (40 nm Ni)/(60 nm Co) (Fig. 2(l)), the depinning does not start with regular DW bands but with nonregular (chaoticlike) pockets/branches of the bands that appear in the phase diagrams. In these cases, the depinning current decreases with increasing segment length.

In the areas of the phase diagrams where the nonregular branching of the bands appear, the DW starts to depin due to the apparition of an antivortex at the boundary between the Ni and Co regions, similar to the depinning from a notch [24,37]. This depinning mechanism is detailed in Fig. 3 for (40-nm Ni)/(80-nm Co) multisegmented nanowire [phase diagram in Fig. 2(m)]. The DW behaves like a string in a tilted washboard potential [22] and cannot be treated as 1D any longer. The position and azimuthal angle depend on the y coordinate. It was shown in Ref. [23] that the azimuthal angle ψ of a 2D DW segment varies as a solution of a Schrodinger-type equation, with the DW anisotropy $K_\perp$ playing the part of the difference between the potential barrier energy and the particle energy. The exponential-like solutions of the Schrodinger equation apply to the azimuthal angle, and a small change in the DW anisotropy at the lower and upper edges induces an exponential increase of ψ at the boundaries. The DW anisotropy changes drastically at the boundary between the Ni and Co regions, therefore a tilting of the azimuthal angle out of the plane is favored. The antivortex appears at the lower edge where the DW center first touches the segment's boundary. The antivortex may be followed by other complex structures (vortex-antivortex pair, half antivortices) depending on the effective exchange strength over the interface [33].

The nucleation and dynamics of the antivortex are more complex here than in the case of a transverse DW movement above the Walker breakdown in an homogeneous strip. As detailed in Figs. 3 and 4 (see movie in Ref. [33]), the DW first pinned in the Ni region starts to move after the application of a current pulse without deformation. After just 20 ps, the DW begins to deform, the lower edge moving faster than the upper edge (contrary to the motion in a homogeneous strip), as shown in the position of the DW center on the top and bottom edges in the first row of Fig. 4. The lower part of the DW center first reaches the Ni/Co boundary, passing slightly

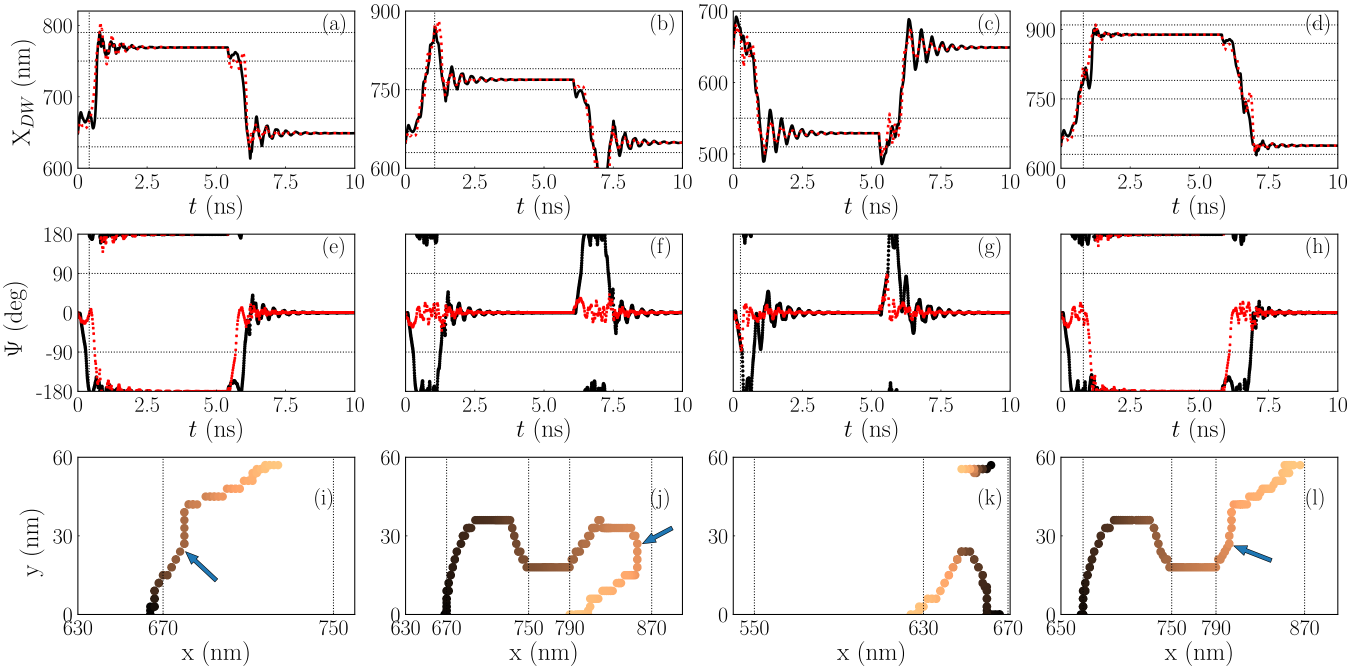

FIG. 4. Time variation of the DW upper (dotted line) and lower (full line) center position (first row) and azimuthal angle (second row) in a 40-nm Ni/80-nm Co multisegmented nanowire. The first column corresponds to a forward followed by a backward pulse with characteristics $t_s = 400$ ps, $j_e = 5.5$ A/μm^2 separated by $t_z = 5$ ns, the second column to forward-backward pulses with characteristics $t_s = 1050$ ps, $j_e = 6.4$ A/μm^2, $t_z = 5$ ns, the third column to forward-backward pulses with characteristics $t_s = 250$ ps, $j_e = 8.5$ A/μm^2, $t_z = 5$ ns, and the last column to to forward-backward pulses with characteristics $t_s = 800$ ps, $j_e = 6.4$ A/μm^2, $t_z = 5$ ns. The last row shows the temporal antivortex trajectory (time variation from dark to lighter colors) with the arrows indicating the current pulse end. The horizontal dotted lines in the first row and the vertical dotted lines in the last row illustrate the Ni regions edges. The vertical dotted lines in the first row pinpoint the current pulse end.

in the Co region and being pulled back (also the upper edge moves back in the same time). The magnetization angle starts turning out of plane in the $-z$ direction at the lower and upper DW edges and along all the DW center line (nanostrip width) as seen in Fig. 3(a). An antivortex is formed at the lower edge with its core polarity along the $-z$ direction (not to be confounded with the transverse DW polarity which is along the $\pm y$ direction), while the magnetization of the upper edge turns gradually along the in-plane direction (after reaching an angle of $-24°$ for $t_s = 400$ ps, $j_e = 5.5$ A/μm^2 or $-32°$ for $t_s = 1050$ ps, $j_e = 6.4$ A/μm^2). For currents above 7.9 A/μm^2, an antivortex can also form at the upper edge, but these cases are fewer and form smaller pocket bands than the ones found below the current values that are discussed here. In the case of a total pulse duration of 0.41 ns for a current amplitude of 5.5 A/μm^2 [Figs. 3(a) and 4, first column], the antivortex moves slowly to the right and up across the strip width with the lower and upper parts of the DW still pinned on the Ni/Co boundary. At the pulse end, the upper edge of the DW moves continuously to the right while the lower edge is pushed in the other direction, strongly deforming the DW. The DW center line has a wavelike dynamical deformation. The antivortex at the center of the wall stays pinned and moves for a short time only in the $+y$ direction. The lower DW edge becomes much larger (still being in the Ni region) and at the same time the upper edge shrinks (being in the Co region). The antivortex begins to move to the right and up (see the trajectory in the bottom row of the Fig. 4), following the upper edge and being attracted to it, and the lower DW edge moves to the right displacing the DW now with opposite polarity to the next Ni region. Bursts of spin waves are ejected along the edges as the antivortex comes out of the nanowire. If the current pulse is applied in the opposite direction, the antivortex will form at the upper edge (image not shown) with a polarity along the $+z$ direction and the DW will travel to the next Ni region to the left, changing its polarity. As discussed below (Sec. III C), the DW displacement with polarity switching is stable at room temperature.

A particularity of the DW motion in the Ni/Co multisegmented nanowire is the possibility of systematic displacement *with or without* polarity switching by changing the pulse characteristics (magnitude and length) for all types of interfaces considered. As observed from the phase diagrams in Fig. 2, when the length of the segments is increased, the homogeneous bands are displaced to the right until they disappear and on the left the chaoticlike pockets of bands appear. In the different pockets corresponding to the +1 state, the antivortex always appears, but it only traverses the nanowire width for low pulse duration. This constitutes a *unique* case, where the motion of a transverse DW between pinning sites takes places with or without polarity switching depending on the pulse length. Figure 3(b) and the second column of Fig. 4 (movie in Ref. [33]) display the case when the pulse length is long enough ($t_s = 1050$ ps, $j_e = 6.4$ A/μm^2 but same behavior for $j_e = 5.5$ A/μm^2) for the antivortex to traverse the next-nearest Ni region completely and come close to the second to the right Ni region before the pulse ends. The antivortex comes out at the lower edge where it entered and the DW is displaced to the next pinning region without polarity switching, contrary to the shorter pulse case. The antivortex strongly deforms when passing the Co/Ni and Ni/Co boundaries with spin-wave emissions (or half antivortices) along the edges. The antivortex moves almost linearly in the Ni and in the middle of the Co regions and shows an inertial displacement after the pulse end continuing in the ± y direction depending on its previous displacement. Therefore, timing the pulse length just right when the antivortex goes up or down in the Co regions (close to the Ni boundaries) will make the antivortex traverse the nanowire width or not and variate the DW polarity. The last column of Fig. 4 shows another possibility of DW polarity switching due to the antivortex traversing the nanowire, where the DW travels to the second pinning Ni region to the right (+2 state). As the pulse ends when the antivortex moves upward, it continues to move until going out at the upper edge, switching the DW polarity.

As shown elsewhere [3,4,38–40], the DW shows automotion (inertial transient displacement) due to the current pulse shape. Here, the automotion appears in some phase diagrams (negative bands) with an example being shown in the third column of Fig. 4. For a pulse width $t_s = 250$ ps and $j_e = 8.5$ A/μm^2, the DW is first pushed to the right (in the direction of the STT) and afterward is pulled back by the potential well. An antivortex is created at the upper edge and a second one at the lower edge, joining across the nanowire width and both moving to the left at the pulse end. The antivortices separate and the upper one is ejected while the lower one enters the nanowire, oscillates in size, emitting spin waves, and comes out of the nanowire. Both antivortices come out on the same edge they entered, while the DW moves to the next Ni region to the left, keeping its polarity.

The motion of a vortex or antivortex in a nanowire can be described by the Thiele equation [30,41],

$$-\mathbf{G}\times\frac{d\mathbf{X}}{dt}-\hat{\mathbf{D}}\frac{d\mathbf{X}}{dt}+\frac{\partial E}{\partial \mathbf{X}}=0, \tag{3}$$

where $\mathbf{X} = (X, Y)$ is the antivortex core position, $E(\mathbf{X})$ is the potential energy of the antivortex, $\mathbf{G}$ is the gyrovector, and $\hat{\mathbf{D}}$ is the damping tensor. The first term of Eq. (3) suggests a Magnus-type force that acts in a perpendicular direction to the antivortex velocity (gyration) pushing it to the edges. The gyrovector is along the z axis and is expressed as $\mathbf{G} = -\frac{2\pi\mu_0 M_s q p t \hat{\mathbf{z}}}{\gamma}$, with q the topological charge ($= -1$ for an antivortex), p the polarization of the antivortex core (± 1 along the z axis), and t the sample thickness. Knowing the potential energy of the antivortex, its motion can be calculated analytically [42,43] and shows a gyrotropic motion under applied magnetic field or current.

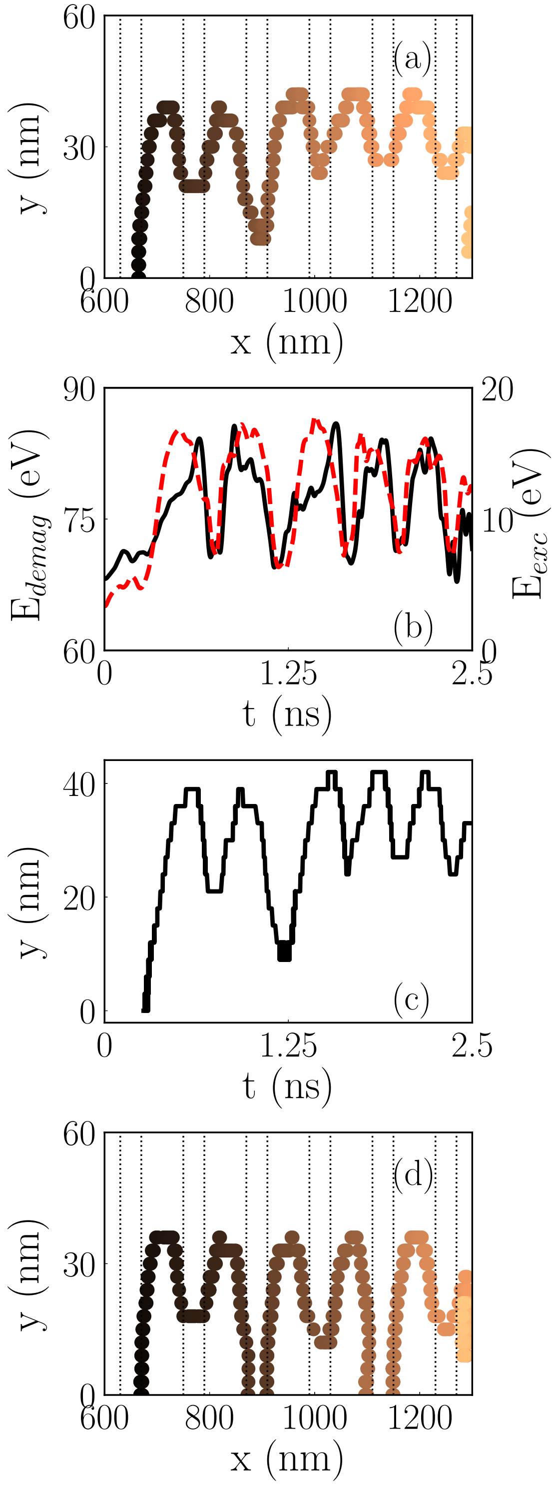

FIG. 5. Temporal antivortex trajectory (time variation from dark to lighter colors) in a 40-nm Ni/80-nm Co multisegmented nanowire for a 5-ns current pulse with magnitude j_e of 5.5 A/μm^2 in (a) and 6.4 A/μm^2 in (d). The temporal evolution of the demagnetizing (full line) and exchange (dashed line) energies and the antivortex y position corresponding to panel (a) are shown in (b) and (c), respectively. The vertical dotted lines in (a) and (d) illustrate the Ni regions edges. The nanowire is 1300 nm long.

In the multisegmented Ni/Co nanowire, the gyrovector is oriented in the $-z$ direction for the initial antivortex. To understand better the motion of the antivortex, a longer current pulse with $t_s = 5$ ns is applied (Fig. 5). The Oersted field created by the current pulse is not taken into account although it may become important for longer pulses, influencing the antivortex motion [42]. The displacement of the antivortex along the nanowire follows a clockwise gyrotropic motion in each Co region crossed. The gyration appears to stop in the Ni regions and to restart again when the antivortex reenters the Co region. The average velocity of the antivortex (not shown) increases to around 400 m/s when approaching a Ni region (on the downward y motion) and decreases to around 250 m/s when the antivotex leaves the Ni region (on the upper y motion). As seen in Fig. 5(b), the demagnetizing energy and the exchange energy have a similar oscillatory behavior each time the antivortex moves across the Co/Ni region correlating with its motion [compare Figs. 5(b) and 5(c)]. The antivortex pursues the potential energy shape, implying that, due to the demagnetizing and exchange energy variation, the gyrotropic motion is lessened whenever the antivortex comes close to a Co/Ni boundary (the demagnetizing field changes signs at each Ni/Co boundary). If the magnitude of the current pulse is too high [see Fig. 5(d)], the gyroforce (which depends on the M_s through the gyrovector and on velocity) is strong enough to push the antivortex out of the wire each second Co region before the antivortex could reach the Ni region. The antivortex is recreated again (comes back into the wire) at the next Ni/Co boundary and this periodic motion continues until it reaches the end of the wire. It should be pointed out that the antivortex does not change its core polarization during its motion in the multisegmented nanowire (for the pulse characteristics used).

B. Influence of material parameters

To control and understand the depinning current in the Ni/Co multisegmented nanowire, we altered the potential energy landscape in which the DW moves by modifying the magnetization, the exchange stiffness, or the anisotropy of the Co regions (along with the damping constant α and the nonadiabatic parameter β) and the effective exchange at the Ni/Co interfaces. While the magnetization of a thin film is measured by magnetometry, the exchange constant is estimated indirectly assuming particular models [27,44], leading to a higher incertainty. Therefore, we varied the exchange constant A on a larger range from 15 to 50 pJ/m (higher values suggested recently [45,46]) and the magnetization M_s between 1300 and 1500 kA/m for the Co regions (details in Ref. [33]). We observed that the depinning current varies oppositely to the depinning field when varying A or M_s, the depinning current decreasing with increasing both A or M_s up to a threshold value. Lowering the magnetization has a higher impact on the potential barrier height for the DW, while the variation of the exchange constant influences more the form of the potential well. In Fig. 6, we present the consequences of the exchange stiffness constant variation (exchange length and DW width scale with $\sqrt{A}$) on the phase diagrams for a multisegmented 40-nm Ni/80-nm Co nanowire. For the lowest exchange constant value [Fig. 6(a)], the regular bands are still visible to the right of the phase diagram but large pockets of disordered bands appear to the left with a large -1 pocket band. Increasing further on the exchange stiffness constant, the regular bands shift to the right of the phase diagram and disappear, leaving only the branching pocket bands that correspond to the antivortex presence. For the largest A value, the pocket bands seem to become more regular for lower current values as the $+1$ band is observed continuously up to a pulse length $t_s = 850$ ps, followed by superior bands (still a $+1$ band branches to higher currents). The dynamics of the DW and the antivortex also changes compared with the case presented above [shown in Fig. 6(c), identical with Fig. 2(n)]. In this case, the branch of the $+1$ band appearing at lower currents (to the left of the phase diagram) does not correspond anymore to the DW movement with polarity change. Inside this branch, the DW moves to the next (+1) Ni region with or without polarity change, as the two different branches seen in Fig. 6(c) (for $A = 28.1$ pJ/m) coalesce. For a current of $j_e = 4.0$ A/μm^2, the DW moves with polarity change up to a pulse length of $t_s = 750$ ps from which the motion takes place without DW polarity change [33]. The antivortex with core polarity in the $-z$ direction that is created at the lower edge traverses the nanowire width faster and disappears at the upper edge in the $+1$ Ni region, while the DW moves to the $+1$ Ni region and remains pinned. Above $t_s = 700$ ps, another antivortex with core polarity in the $+z$ direction is formed at the upper edge in the $+1$ Ni region and, for pulses between 750 ps and 850 ps, traverses the nanowire width almost vertically in the Ni region (with the DW staying pinned) changing the DW polarity to the initial one ($+y$ direction). For longer pulses, the second antivortex moves toward the $+2$ Ni region before going out of the sample, displacing the DW to the $+2$ Ni region. The DW motion with polarity change is still stable at room temperature (see next section) even for the increased stiffness constant.

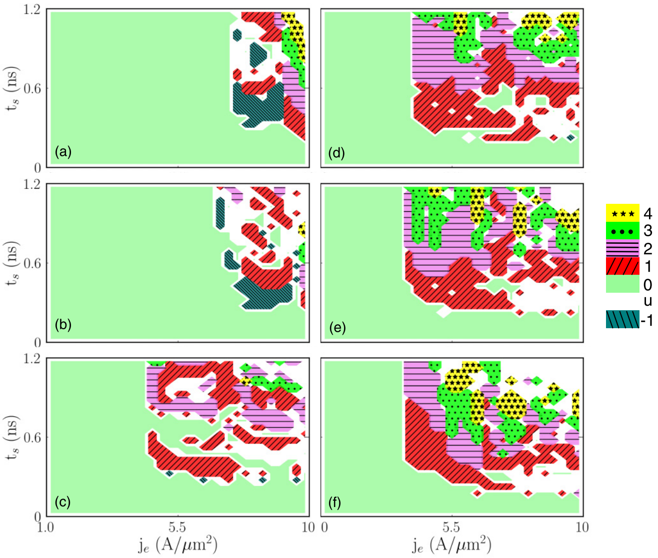

FIG. 6. Micromagnetic phase diagrams of DW motion under a periodic current pulse in a multisegmented 40-nm Ni/80-nm Co nanowire at $T = 0$ K. Only exchange stiffness constant A is varied for the Co regions from 15 pJ/m (a) to 20 pJ/m (b), 28.1 pJ/m (c), 35 pJ/m (d), 40 pJ/m (e), and 50 pJ/m (f). The observed DW motion is classified in bands numbered as follows: positive bands correspond to the DW moving in the direction of the electron flow, negative numbers to the DW moving contrary to the electron flow, zero state correspond to the DW staying pinned at initial position, and u to the unintended states in which the DW does not come back to the initial state after the periodic pulse.

When the effective exchange energy is lowered, the DW motion with polarity change still arises, with the antivortex moving along the Ni/Co interface and reversing the polarity of the DW. The bandlike states become larger and more ordered and the systematic DW motion is more stable

[33]. When the effective inter-region exchange is increased (considering the same value on both sides of the interface), the antivortex traverses the nanowire width faster and other complex structures appear as vortex-antivortex pairs or half-antivortices along the edges. The state bands are intermixed and less regular, but the DW motion with polarity changing still occurs depending on the pulse characteristics.

When varying the magnitude of the magnetocristalline anisotropy constant K_u for the Co segments, the phase diagram is modified greatly [33]. For a 40-nm Ni/80-nm Co wire, when the anisotropy constant is lowered to a value of 5×10^4 J/m^3, from 4.5×10^5 J/m^3, the regular bands are still visible with small band pockets to the left, almost identical to the case of shorter Co segments [of 60 nm, shown in Fig. 2(l)]. The states/bands are displaced to the left (lower currents) in the phase diagram. Even when the the anisotropy constant of the Co regions is turned off (equal to zero as in the Ni regions), the phase diagram is similar to the one of the reduced anisotropy constant with band pockets between 3.1 and 8.2 A/μm^2 and regular bands above. However, in the band pockets, the DW motion with polarity switching does not happen for all the points in the same band pocket and pairs of vortex-antivortex can enter the nanowire even for low currents, making the DW motion with or without polarity switching unstable. When the anisotropy constant is increased to a value of 1×10^6 J/m^3, the regular bands and the pocket bands almost disappear, as the DW is highly distorted, being pinned at the boundary of the Ni/Co regions and transforming in several perpendicular DWs when moving across the Co regions (uniaxial anisotropy higher than demagnetizing energy). The systematic DW displacement is no longer stable in this case.

Altering the pulse shape, varying the rise time or the fall time has the same impact on the phase diagrams as for a notched nanowire [3], displacing the states at higher currents and does not improve the dynamics discussed here.

To be able to compare to other real materials, whose parameters were already measured, we replace the Co regions with a $Co_{50}Ni_{50}$ alloy with the following parameters: $M_s = 1070$ kA/m, $A = 22.7$ pJ/m, and $K_u = 7.5 \times 10^4$ J/m^3 [44]. The damping constant α is varied between the values of Ni and Co [47,48]. Alloying the Co regions with Ni decreases the DW potential barrier between the regions and thus it should lower the depinning current. The results are presented in Fig. 7. For a 30-nm Ni/50-nm $Co_{50}Ni_{50}$ multisegmented nanowire [Fig. 7(a)], the depinning current decreases to 1.9 A/μm^2 from 2.8 A/μm^2 for the case of pure Co regions [Fig. 2(f)], while the bands become larger and more regular. The same situation is observed for the 20-nm Ni/60-nm $Co_{50}Ni_{50}$ multisegmented nanowire, with the depinning current being 2.2 A/μm^2 (as compared to 3.4 A/μm^2 for pure Co). Varying the segment length, we observe that the pocketlike bands due to the presence of the antivortex appear for longer segment lengths. The regular bands are still visible for the 40-nm Ni/80-nm $Co_{50}Ni_{50}$ mulstisegmented nanowire (Fig. 7(c)), even when a lower damping parameter (equal to the one of Co) is used for $Co_{50}Ni_{50}$ segments (Fig. 7(d)). In this case, for both damping parameters, the same behavior is observed in the pocket bands as for the Ni/Co multisegmented wire: For the lower t_s pockets of the +1 band, the DW changes polarity when moving to the +1 pinning site while, for larger t_s pockets of the +1 band, the DW does not change its polarity when moving to the next pinning site (the antivortex enters and comes out of the nanowire on the lower edge).

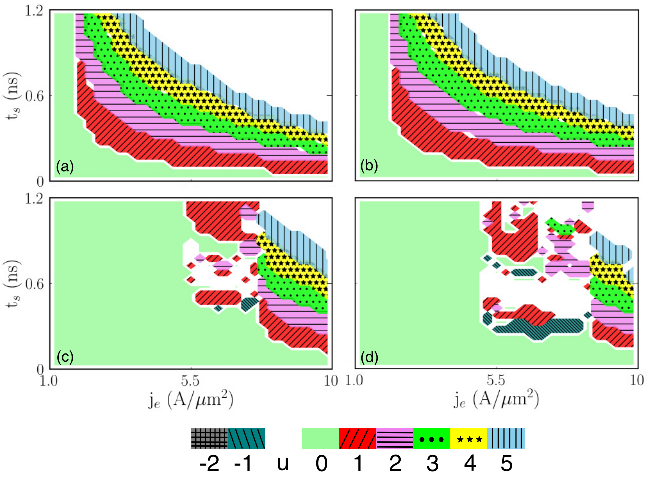

FIG. 7. Micromagnetic phase diagrams of DW motion under a periodic current pulse in a multisegmented $Ni/Co_{50}Ni_{50}$ nanowire at $T = 0$ K. The length of the regions varies as (a), 30-nm Ni/50-nm $Co_{50}Ni_{50}$; (b), 20-nm Ni/60-nm $Co_{50}Ni_{50}$; (c), (d) 40-nm Ni/80-nm $Co_{50}Ni_{50}$. From (a)–(c), $\alpha = 0.05$ and $\beta = 2\alpha$ for both region types, while in (d) $\alpha_{Co_{50}Ni_{50}} = 0.005$. The observed DW motion is classified in bands numbered as follows: positive bands correspond to the DW moving in the direction of the electron flow, negative numbers to the DW moving contrary to the electron flow, zero state correspond to the DW staying pinned at initial position, and u to the unintended states in which the DW does not come back to the initial state after the periodic pulse.

C. Temperature dependence

The temperature is taken into account by introducing a stochastic thermal field in the effective field term of the LLG equation in both the precession and damping terms [49]. The effect of temperature was computed micromagnetically mainly for the +1 band on 100 realizations per point. A symmetric current pulse ($t_r = t_f = 5$ ps) was applied after an initial relaxation time of 5 ns, followed by another relaxation time of 5 ns. These results are valid at low temperatures compared to the Curie temperature of materials, as the saturation magnetization is considered constant. At larger temperatures, the alternatives are the Landau-Lifschitz-Bloch equation or an atomistic model [50,51].

In Fig. 8, the probability distributions at $T = 293$ K for positioning the DW to the nearest notch (+1 band) for different Co/Ni or $Co_{50}Ni_{50}$/Ni multisegmented nanowires are shown. The probability distribution for a regular +1 band (no antivortex present) is shown in the first two columns, while in the last column the probability distribution when the antivortex appears and traverses the nanowire. In Fig. 8(a), for a 30-nm Ni/50-nm Co nanowire, the maximum of the probability distribution is of 87% obtained for a pulse with $t_s = 150$ ps and $j_e = 6.1$ A/μm^2. The maximum of the probability distribution increases to 96% for the multisegmented 20-nm

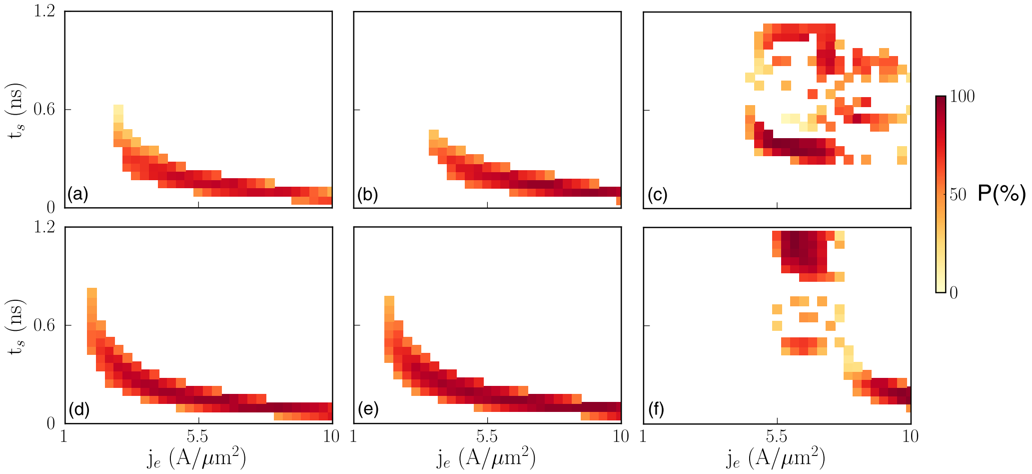

FIG. 8. Probability of DW motion in +1 bands at $T = 293$ K for a multisegmented nanowire of Ni and Co or $Co_{50}Ni_{50}$ regions: (a) 30-nm Ni/50-nm Co, (b) 20-nm Ni/60-nm Co, (c) 40-nm Ni/80-nm Co, (d) 30-nm Ni/50-nm $Co_{50}Ni_{50}$, (e) 20-nm Ni/60-nm $Co_{50}Ni_{50}$, and (f) 40-nm Ni/80-nm $Co_{50}Ni_{50}$.

Ni/60-nm Co nanowire [Fig. 8(b)], obtained for the pulse characteristics $j_e = 9.1$ A/μm^2 and $t_s = 100$ ps. The maximum probability increases to 100% for the multisegmented 40-nm Ni/50-nm Co nanowire (image not shown) at the same pulse characteristics. In the case of a Ni/$Co_{50}Ni_{50}$ wire, the maximum of the distribution probability is of 96% for $j_e = 8.2$ A/μm^2 and $t_s = 100$ ps for 30-nm Ni/50-nm $Co_{50}Ni_{50}$ segmented wire [Fig. 8(d)], and of 97% for $j_e = 6.1$ A/μm^2 and $t_s = 150$ ps for 20-nm Ni/60-nm $Co_{50}Ni_{50}$ segmented wire [Fig. 8(e)].

In the case of DW displacement with polarity change, the maximum of the probability distribution is of 100% for 40-nm Ni/80-nm Co multisegmented nanowires [Fig. 8(d)] for several points centered on $j_e = 5.5$–6.1 A/μm^2 and $t_s = 350$–400 ps (also obtained for other values of effective exchange). This indicates that the systematic DW motion with polarity change is stable at room temperature in a reasonable parameter range and can lead to practical applications. For the regular DW displacement without polarity change, the maximum of the probability distribution is reached for $j_e = 6.4$ A/μm^2 and $t_s = 1050$ ps and is of 82% in the same multisegmented nanowire. The motion with polarity change is more stable at room temperature than the motion without for the chosen parameters. The maximum probability diminishes to 75% in the second band and to 28% for the -1 band (not shown). The 100% maximum probability for DW motion with probability change is also realized for the same multisegmented wire with an increased stiffness constant A of 50 pJ/m for the Co regions for slightly lower pulse values ($j_e = 5.2$–5.5 A/μm^2 and $t_s = 350$–400 ps). A high probability of DW displacement (96%) is also obtained for a 40-nm Ni/70-nm Co wire at $j_e = 5.5$ A/μm^2 and $t_s = 400$ ps for the +1 band, corresponding to polarity changing DW motion, similarly as above. On the contrary, for the 40-nm Ni/80-nm $Co_{50}Ni_{50}$ segmented wire [Fig. 8(f)], the maximum rate of success of 100% is realized for the DW motion without polarity change around $j_e = 6.1$ A/μm^2 and t_s between 1100–1150 ps, while the success rate decreases to 68% for the polarity changing motion ($j_e = 6.4$ A/μm^2 and $t_s = 500$ ps). This behavior can be understood by the larger pocket of the +1 band (at lower t_s), corresponding to polarity changing motion, for the Co/Ni wire than for the Ni/$Co_{50}Ni_{50}$ wire.

IV. DISCUSSION AND CONCLUSIONS

A multisegmented Ni/Co nanowire constitutes a particular case in which a transverse magnetic DW can be displaced systematically between well-defined pinning sites (Ni segments), with or without polarity switching between initial and final positions. This system brings an additional degree of freedom (the DW polarity) to the DW motion compared to the homogeneous nanowire with artificial constrictions studied extensively [3]. Depending on the particular geometric dimensions of the segments and material parameters as discussed below, the DW can be displaced with polarity flip controlled by the current pulse characteristics. The DW polarity flip is primarily due to the birth and propagation of an antivortex along the DW width similar to the DW motion above the Walker breakdown in homogeneous nanostrips. The antivortex is created at the boundary between the Ni/Co regions and has in part the expected gyrotropic motion governed by the complex potential along the wire. The polarity switch is determined by the current pulse length (and magnitude), the antivortex keeping its previous motion direction after the pulse end. The antivortex can be displaced long distances along the multisegmented nanowire having a sinusoidal motion depending on the boundary conditions and effective exchange.

Several parameters play an important role in the emergence of complex textures in the Ni/Co multisegmented nanowire. The total energy of the system comprises the exchange energy, the anisotropy energy which for Co segments is given by the effective anisotropy constant $K_{\mathrm{eff}} = K_u - N_z\mu_0 M_s^2/2$, the effective DW transverse anisotropy $K_\perp \sin^2\psi$ [52] where $K_\perp = K_y - K_x$ for the Co regions with perpendicular anisotropy and $K_\perp = K_z - K_y$ for the Ni regions with in-plane anisotropy (K_i—effective anisotropy constants) and the pinning energy. It was shown previously that a step in the anisotropy (K_{eff}) [12] pins the DW and that the depinning field depends on the anisotropy step. Under an applied polarized current, the stable Neel wall in the Ni region will start to move and tilt (increasing ψ). The rotation anisotropy barrier to the transition to a Bloch wall depends on the rotation anisotropy constant $K_\perp$, the DW width Δ, and the azimuthal angle ψ [13]. This rotation anisotropy barrier suppresses the tilting of the DW when $K_\perp$ is large [22,23]. In the studied case, at the Ni/Co boundary there is a large fluctuation in $K_\perp$ due to the large variation in the saturation magnetization and the suppression of the tilting no longer applies. The DW transverse anisotropy constant $K_\perp$ fluctuation is a main ingredient that leads to the birth of an antivortex and to the DW motion with polarity switching. We also observed that, for the segment lengths studied, the antivortex starts to emerge when the transverse anisotropy $K_\perp$ changes sign for the Co regions. In the opposite case, when the rotation anisotropy barrier is too low (increasing K_u in Co) the DW starts to rotate and transforms from Neel to Bloch wall when moving, leading to a nonreliable systematic movement between pinning regions. Even though the antivortex emerges without a perpendicular magnetocrystalline anisotropy (PMA) present ($K_u = 0$ in Co), the presence of a moderate PMA favors the emergence and stability of a singular antivortex at lower currents and supports the large +1 band pockets with or without a homogeneous DW polarity switching. Another principal ingredient is the exchange energy variation between segments, as detailed in part in Fig. 6: A moderate exchange constant A preserves the different +1 band pockets while an increase barrier will collapse the different pockets and reduce the possibility of DW motion with or without polarity switching. A low effective exchange stiffness at the Ni/Co interfaces stabilizes the DW motion and diminishes the apparition of other complex textures, leading to larger state bands [33].

In the case of only an adiabatic STT (nonadiabatic parameter $\beta = 0$ in all segments), an antivortex still forms (see figure in Ref. [33]), but for 40-nm Ni/80-nm Co segments, the lower and upper +1 band pockets collapse and form only one band with very few states without DW polarity motion reducing the applications.

The DW motion with polarity switching between neighboring pinning segments (+1 band) is room-temperature compatible as the success rate is 100% in a reasonable current range depending on the segment's length. For 40-nm-long Ni segments, the success rate is only 76% for DW motion with polarity flip and 71% without polarity flip for 60-nm Co segments. The maximum probability increases systematically with the Co segment length, being of 96% and 88% with and without polarity switch for 70-nm Co segments and up to 100% and 92% for 90-nm Co segments. The room-temperature stability paves the way for possible memory applications.

Our results predict that the best possible implementation for memory devices (like the racetrack memory) is obtained for Ni segments with widths comparable with the DW width having neighboring segments with materials parameters not very different from those of Ni having a lower variation at the interfaces. In this respect, a Co-Ni alloy with a magnetization, exchange stiffness, and anisotropy closer to the Ni values (and a lowered effective exchange at the interface) reduce the apparition of complex textures (like antivortices or vortices) and stabilize the DW motion, leading to lower depinning currents and larger bands, increasing the range of reliable systematic DW displacement. This could be the case in real structures, where the grain boundaries are far from perfect.

In summary, transverse DW motion with or without polarity switching was shown to occur in multisegmented Ni/Co nanowires depending only on the current pulse shape. The polarity switching is mainly due to the emergence of complex textures that traverse the nanowire width. The motion is room-temperature compatible and can be engineered by alloying. The additional degree of freedom in the DW motion can open the way for logical or memory devices based on the information encoding into the magnetization direction of a DW.

ACKNOWLEDGMENTS

This work was granted access to the HPC resources of Aix-Marseille Université financed by the project Equip@Meso (ANR-10-EQPX-29-01) of the program Investissements d'Avenir supervised by the Agence Nationale pour la Recherche.

---

[1] D. A. Allwood, G. Xiong, C. C. Faulkner, D. Atkinson, D. Petit, and R. P. Cowburn, Science **309**, 1688 (2005).
[2] S. S. P. Parkin, M. Hayashi, and L. Thomas, Science **320**, 190 (2008).
[3] A. Pivano and V. O. Dolocan, Phys. Rev. B **96**, 224431 (2017).
[4] A. Pivano and V. O. Dolocan, Phys. Rev. B **101**, 014438 (2020).
[5] D. Petit, A.-V. Jausovec, D. Read, and R. P. Cowburn, J. Appl. Phys. **103**, 114307 (2008).
[6] D. Petit, A.-V. Jausovec, H. T. Zeng, E. Lewis, L. O'Brien, D. Read, and R. P. Cowburn, Phys. Rev. B **79**, 214405 (2009).
[7] E. Martinez, L. Lopez-Diaz, O. Alejos, L. Torres, and M. Carpentieri, Phys. Rev. B **79**, 094430 (2009).
[8] H. Y. Yuan and X. R. Wang, Phys. Rev. B **89**, 054423 (2014).
[9] V. O. Dolocan, Appl. Phys. Lett. **105**, 162401 (2014).
[10] F. Lofink, A. Philippi-Kobs, M. R. Rahbar Azad, S. Hankemeier, G. Hoffmann, R. Fromter, and H. P. Oepen, Phys. Rev. Appl. **8**, 024008 (2017).
[11] A. Vogel, S. Wintz, T. Gerhardt, L. Bocklage, T. Strache, Mi-Y. Im, P. Fischer, J. Fassbender, J. McCord, and G. Meier, Appl. Phys. Lett. **98**, 202501 (2011).
[12] J. H. Franken, M. Hoeijmakers, R. Lavrijsen, and H. J. M. Swagten, J. Phys.: Condens. Matter **24**, 024216 (2012).
[13] T. Gerhardt, A. Drews, and G. Meier, J. Phys.: Condens. Matter **26**, 206001 (2014).
[14] E. Berganza, M. Jaafar, C. Bran, J. A. Fernandez-Roldan, O. Chubykalo-Fesenko, M. Vazquez, and A. Asenjo, Sci. Rep. **7**, 11576 (2017).
[15] Yu. P. Ivanov, A. Chuvilin, S. Lopatin, and J. Kosel, ACS Nano **10**, 5326 (2016).
[16] B. Leighton, O. J. Suarez, P. Landeros, and J. Escrig, Nanotechnology **20**, 385703 (2009).
[17] C. Bran, E. Berganza, J. A. Fernandez-Roldan, E. M. Palmero, J. Meier, E. Calle, M. Jaafar, M. Foerster, L. Aballe, A. Fraile

Rodriguez, R. P. del Real, A. Asenjo, O. Chubykalo-Fesenko, and M. Vazquez, ACS Nano **12**, 5932 (2018).
[18] C. Bran, Yu. P. Ivanov, J. Kosel, O. Chubykalo-Fesenko, and M. Vazquez, Nanotechnology **28**, 095709 (2017).
[19] T. da Camara Santa Clara Gomes, F. Abreu Araujo, L. Piraux, Sci. Adv. **5**, eaav2782 (2019).
[20] *Magnetic Nano- and Microwires*, edited by M. Vazquez (Elsevier, Oxford, 2020).
[21] Yu. P. Ivanov, L. G. Vivas, A. Asenjo, A. Chuvilin, O. Chubykalo-Fesenko, and M. Vazquez, Europhys. Lett. **102**, 17009 (2013).
[22] R. A. Duine and C. M. Smith, Phys. Rev. B **77**, 094434 (2008).
[23] J. Ryu, S.-B. Choe, and H.-W. Lee, Phys. Rev. B **84**, 075469 (2011).
[24] H. Y. Yuan and X. R. Wang, J. Magn. Magn. Mater. **368**, 70 (2014).
[25] S. Zhang and Z. Li, Phys. Rev. Lett. **93**, 127204 (2004).
[26] R. D. McMichael and M. J. Donahue, IEEE Trans. Magn. **33**, 4167 (1997).
[27] C. A. F. Vaz, J. A. C. Bland, and G. Lauhoff, Rep. Prog. Phys. **71**, 056501 (2008).
[28] A. Vansteenkiste, J. Leliaert, M. Dvornik, M. Helsen, F. Garcia-Sanchez, and B. Van Waeyenberge, AIP Adv. **4**, 107133 (2014).
[29] M. J. Donahue and D. G. Porter, OOMMF User's Guide Version 1.0. (National Institute of Standards and Technology, Gaithersburg, MD, 1999), http://math.nist.gov/oommf/.
[30] A. Thiaville and Y. Nakatani, in *Spin Dynamics in Confined Magnetic Structures III*, edited by B. Hillebrands and A. Thiaville (Springer, Berlin, 2006).
[31] O. Boulle, G. Malinowski, and M. Kläui, Mater. Sci. Eng. R **72**, 159 (2011).
[32] M. E. Lucassen, H. J. van Driel, C. M. Smith, and R. A. Duine, Phys. Rev. B **79**, 224411 (2009).
[33] See Supplemental Material at https://link.aps.org/supplemental/10.1103/PhysRevB.103.054435 for details of parameters influence on phase diagram.
[34] M. J. Donahue and D. G. Porter, Physica B **343**, 177 (2004).
[35] R. Skomski, J. Phys.: Condens. Matter **15**, R841 (2003).
[36] T. Schrefl and J. Fidler, J. Magn. Magn. Mater. **177**, 970 (1998).
[37] H. Y. Yuan and X. R. Wang, Phys. Rev. B **92**, 054419 (2015).
[38] A. Thiaville, Y. Nakatani, F. Piechon, J. Miltat, and T. Ono, Eur. Phys. J. B **60**, 15 (2007).
[39] J. Y. Chauleau, R. Weil, A. Thiaville, and J. Miltat, Phys. Rev. B **82**, 214414 (2010).
[40] B. Krüger, D. Pfannkuche, M. Bolte, G. Meier, and U. Merkt, Phys. Rev. B **75**, 054421 (2007).
[41] A. A. Thiele, Phys. Rev. Lett. **30**, 230 (1973).
[42] A. Drews, B. Kruger, M. Bolte, and G. Meier, Phys. Rev. B **77**, 094413 (2008).
[43] K.-S. Lee and S.-K. Kim, Appl. Phys. Lett. **91**, 132511 (2007).
[44] P. Talagala, P. S. Fodor, D. Haddad, R. Naik, L. E. Wenger, P. P. Vaishnava, and V. M. Naik, Phys. Rev. B **66**, 144426 (2002).
[45] M. D. Kuzmin, K. P. Skokov, L. B. Diop, I. A. Radulov, and O. Gutfleisch, Eur. Phys. J. Plus **135**, 301 (2020).
[46] R. Moreno, R. F. L. Evans, S. Khmelevskyi, M. C. Munoz, R. W. Chantrell, and O. Chubykalo-Fesenko, Phys. Rev. B **94**, 104433 (2016).
[47] K. Gilmore, Y. U. Idzerda, and M. D. Stiles, Phys. Rev. Lett. **99**, 027204 (2007).
[48] S. Mankovsky, D. Ködderitzsch, G. Woltersdorf, and H. Ebert, Phys. Rev. B **87**, 014430 (2013).
[49] J. Leliaert, J. Mulkers, J. De Clercq, A. Coene, M. Dvornik, and B. Van Waeyenberge, AIP Adv. **7**, 125010 (2017).
[50] D. A. Garanin, Phys. Rev. B **55**, 3050 (1997).
[51] N. Kazantseva, D. Hinzke, U. Nowak, R. W. Chantrell, U. Atxitia, and O. Chubykalo-Fesenko, Phys. Rev. B **77**, 184428 (2008).
[52] S.-W. Jung, W. Kim, T.-D. Lee, K.-J. Lee, and H.-W. Lee, App. Phys. Lett. **92**, 202508 (2008).